Clinical Neurophysiology 125 (2014) 2016–2023

Contents lists available at ScienceDirect

Clinical Neurophysiology

journal homepage: www.elsevier.com/locate/clinph

Experimental observation of a theoretically predicted nonlinear sleep spindle harmonic in human EEG

R.G. Abeysuriya [a,b,c,*], C.J. Rennie [a,b], P.A. Robinson [a,b,c], J.W. Kim [a,b,c]

[a] School of Physics, University of Sydney, New South Wales 2006, Australia
[b] Brain Dynamics Center, Sydney Medical School – Western, University of Sydney, Westmead, New South Wales 2145, Australia
[c] Center for Integrated Research and Understanding of Sleep, 431 Glebe Point Rd, Glebe, New South Wales 2037, Australia

ARTICLE INFO

Article history:
Accepted 24 January 2014
Available online 10 February 2014

Keywords:
EEG
Neurophysiology
Sleep spindles
Neural field theory

HIGHLIGHTS

- We analyze EEG data to examine the properties of a spindle harmonic oscillation.
- The harmonic occurs at twice the frequency of the spindle, scales nonlinearly in power, and is accompanied by high bicoherence.
- The spindle harmonic is consistent with predictions made by a theoretical neural field model of the brain explaining the generation of the harmonic.

ABSTRACT

Objective: To investigate the properties of a sleep spindle harmonic oscillation previously predicted by a theoretical neural field model of the brain.
Methods: Spindle oscillations were extracted from EEG data from nine subjects using an automated algorithm. The power and frequency of the spindle oscillation and the harmonic oscillation were compared across subjects. The bicoherence of the EEG was calculated to identify nonlinear coupling.
Results: All subjects displayed a spindle harmonic at almost exactly twice the frequency of the spindle. The power of the harmonic scaled nonlinearly with that of the spindle peak, consistent with model predictions. Bicoherence was observed at the spindle frequency, confirming the nonlinear origin of the harmonic oscillation.
Conclusions: The properties of the sleep spindle harmonic were consistent with the theoretical modeling of the sleep spindle harmonic as a nonlinear phenomenon.
Significance: Most models of sleep spindle generation are unable to produce a spindle harmonic oscillation, so the observation and theoretical explanation of the harmonic is a significant step in understanding the mechanisms of sleep spindle generation. Unlike seizures, sleep spindles produce nonlinear effects that can be observed in healthy controls, and unlike the alpha oscillation, there is no linearly generated harmonic that can obscure nonlinear effects. This makes the spindle harmonic a good candidate for future investigation of nonlinearity in the brain.

1. Introduction

One of the key indicators of sleep stage 2 is the presence of sleep spindles – short bursts of 12–15 Hz EEG activity lasting around 0.5–1 s, as shown in Fig. 1 (Contreras et al., 1997; Niedermeyer and Lopes da Silva, 1999). Much new research focuses on the roles spindles may play in learning and memory formation (Schabus et al., 2004; Clemens et al., 2005; Saletin et al., 2011), but the mechanisms of spindle generation still require some clarification.

Neural field theory has proved to be a powerful technique for constructing relatively simple physiological models of the brain that reproduce a wide variety of EEG and many other experimental results. We have developed a neural field corticothalamic model of the brain (Robinson et al., 2001, 2002, 2004, 2005; Rowe et al.,

* Corresponding author at: School of Physics, University of Sydney, New South Wales 2006, Australia. Tel.: +61 2 9036 7274.
E-mail address: r.abeysuriya@physics.usyd.edu.au (R.G. Abeysuriya).

http://dx.doi.org/10.1016/j.clinph.2014.01.025
1388-2457/

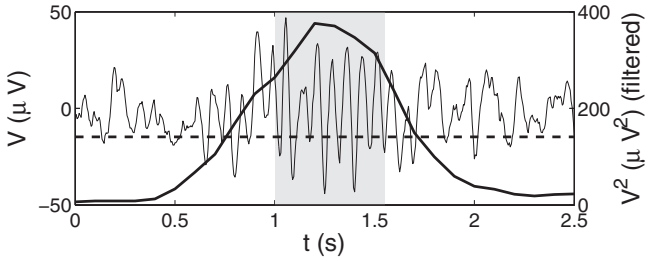

Fig. 1. EEG time series from Cz electrode (thin line) showing an automatically identified sleep spindle, occurring in the gray shaded area. The DC component has been removed from the data. The squared and downsampled time series is the bell-shaped curve (thick line) displayed using the vertical axis on the right side. The dashed horizontal line is the detection threshold.

2004) and used it to investigate the alpha rhythm (Robinson et al., 2003; O'Connor and Robinson, 2004), age-related changes to the physiology of the brain (van Albada et al., 2010), evoked response potentials (Rennie et al., 2002), and other phenomena (Robinson et al., 2003; Breakspear et al., 2006; Rowe et al., 2004). Our model produces sleep spindles due to mutual feedback between thalamic relay nuclei and the thalamic reticular nucleus, which has also been proposed on physiological grounds as a mechanism for sleep spindle generation (von Krosigk et al., 1993; Steriade and Sejnowski, 1993; McCormick and Bal, 1997).

Using our model, we recently predicted the existence of a sleep spindle harmonic arising from nonlinear effects in the thalamic relay nuclei within the above feedback loop (Abeysuriya et al., 2014). In that study, we also verified the existence of the spindle harmonic in sample experimental data, and made testable predictions to verify the nonlinear origin of the spindle harmonic. In the present work, we analyze normal healthy adult human EEGs to test the predicted properties of the spindle harmonic. In particular, we test the predictions that the frequency of the spindle harmonic should be almost exactly double the frequency of the sleep spindle, and that the power in the spindle harmonic should scale quadratically with the power of the sleep spindle oscillation.

A nonlinear relationship between the spindle and its harmonic would lead to phase relationships between the two peaks, which can be measured by examining the bicoherence. Bicoherence at the spindle frequency itself has been observed in previous studies, most notably in Akgül et al. (2000) which found strong bicoherence at the spindle frequency. That study presented EEG power spectra that showed some evidence of a spindle harmonic, although this was not discussed there. Other studies have observed bicoherence at the spindle frequency as well, with both Fourier (Venkatakrishnan et al., 2010; Morimoto et al., 2006; Hayashi et al., 2007) and wavelet analysis (Li et al., 2011). A spindle harmonic has been observed under anesthesia in opiate-dependent patients (Wolter et al., 2006), which was recognized as being an oscillation associated with spindle activity occurring at twice the spindle frequency, but it was not identified as a harmonic and its properties were not investigated.

In Section 2, we outline the processing required to observe the sleep spindle harmonic using full-night polysomnograms, review our model predictions, and outline the procedures used to analyze the experimental data. Results are provided in Section 3, and the interpretation and significance of our findings are discussed in Section 4.

2. Method

In this section, we review the methods used to process and analyze the sleep spindle data to quantify the spindle harmonic, and the theoretical predictions made by our model that we test in Section 3.

2.1. Recording and isolating spindles

Polysomnograms (PSGs) from 9 healthy controls (age 25–36, 8 male 1 female) were gathered overnight, as described in D'Rozario et al. (2013). Recordings were made using an Alice-4 system (Respironics, Murraysville PA, USA) at the Woolcock Institute of Medical Research, with 6 EEG channels sampled at 200 Hz and electrodes positioned according to the International 10–20 system. For this study, only the Cz electrode was examined, referenced to M1. A notch filter at 50 Hz (as provided by the Alice-4 system) was used to remove mains voltage interference. No other hardware filters were used.

Sleep EEG power spectra are often calculated from relatively long time series (such as 30 s epochs), which combine periods with and without spindles. This type of spectrum is shown in Fig. 2 for a healthy control subject in S2 sleep. A strong peak is evident at ≈ 13 Hz, corresponding to spindle activity, but the contribution from spindle activity is combined with a contribution from background S2 sleep, which is relatively smooth. This makes the spindle peak weaker relative to the background activity because the spindle is only present some of the time. In order to investigate the EEG properties of spindles themselves, it is necessary to separate the sleep spindles from background sleep periods before calculating the power spectrum. Doing so increases the relative strength of the spindle peak, and also reveals weaker features that are otherwise obscured.

An automated spindle detection algorithm is used to identify spindle events in the EEG data. Detection is accomplished by first selecting 30s epochs in the data that have been manually scored as sleep stages 2–4. A 11–16 Hz bandpass FIR filter is applied to the Cz electrode voltage for each epoch. The filtered data are then squared and downsampled to 10 Hz by taking a centered average with a window length of 1 s. An example of the resulting signal is shown in Fig. 1. This processed signal is large when sleep spindles are present.

Next, the epochs are concatenated and the median $\widetilde{V}$ and standard deviation σ of the squared downsampled voltage are computed. The threshold voltage V_t for spindle detection in the downsampled time series is set to $\widetilde{V} + 3\sigma$, and is therefore different for each subject, taking into account differences in physiology and in recording setup. The threshold voltage for the subject in Fig. 1 is shown as a horizontal line. If more than 10 consecutive points in the downsampled time series have a voltage exceeding

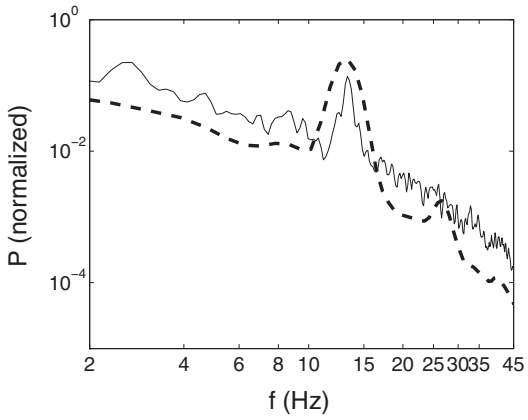

Fig. 2. Comparison of normalized EEG power spectra for 30 seconds of typical S2 sleep when spindle activity was present (solid line), and the power spectrum after isolating spindle activity (dashed line). The spectrum after isolating spindles exhibits a larger, wider spindle peak, and also shows a secondary peak at approximately double the frequency of the first. From Abeysuriya et al. (2014) with permission from Elsevier.

the threshold, that block is identified as a candidate spindle event. The leading and trailing 0.25 s of the block are removed to approximately account for the rise and fall time of the spindle. The final output is a set of spindle start and stop times identifying when sleep spindles occurred, which are used to select segments of data from the raw signal. This process is shown schematically in Fig. 3 and an example of the results is shown in Fig. 2.

2.2. Power spectrum and artifact removal

The next step in the data analysis is to compute the Fourier transform of each detected spindle event, which was performed using a Hamming window (Hamming, 1983). As each event has a different duration, zero padding is applied to each spindle event to ensure that the transforms all contain the same number of data points. A typical spindle event is around 0.5–1 s in duration, and for each subject they are padded to either 256 or 512 samples depending on the length of the longest detected spindle for that subject. This allows the power spectrum for each spindle event to be calculated for the same frequency values for each subject without requiring further interpolation or smoothing.

Due to the short duration of the spindle events, each individual spectrum has a large amount of noise. Unweighted averaging over all such spectra is performed for each subject to produce a smooth spectrum representative of sleep spindles for that subject.

Some of the automatically identified events correspond to artifacts rather than spindles and including these artifacts greatly alters the power spectrum. Typical artifact rejection schemes are designed to identify artifacts in long, continuous recordings, whereas our data consists of a set of very short recordings. Hence we take a different approach to detect artifacts in our data while allowing for individual subject differences.

In our approach, artifacts are identified by first averaging all of the candidate spindle power spectra. The power spectrum for each candidate spindle is then compared to the averaged spectrum. The difference between the two corresponds to how greatly a given spindle event differs from typical spindle activity for that subject, and this power difference is quantified by integrating the squared difference between the spectra. Because the individual spectra are noisy, they all differ from the average spectrum by some amount, but artifacts differ from the average spectrum by significantly more than can be accounted for by noise. Therefore, artifacts can be identified as outliers in terms of the squared difference. This procedure relies on the assumption that there are considerably more spindle events than artifacts, which is typically the case, although the quality of the data must be examined prior to using this method.

We detect the artifacts using the generalized extreme Studentized deviate method for outlier detection (yu et al., 2004; Rosner, 1983) which is suitable for problems where there are multiple outliers and the number of outliers is not known in advance. The artifacts are identified at a significance level of $\alpha = 0.05$ and the maximum amount of artifacts searched for is limited to 20% of the data set. In our data set around 10–15% of candidate spindles for each subject are identified as artifacts.

The result of this artifact rejection scheme is illustrated in Fig. 4. Without removing the artifacts, the spindle harmonic is significantly obscured by artifacts. The artifact rejection scheme removes 13 of the 86 candidate spindle events for this particular subject, resulting in a clear spindle harmonic and removal of the non-spindle features at very high frequencies visible in Fig. 4.

2.3. Frequency relationship

In our modeling work, we predicted that a spindle harmonic will occur at a frequency twice that of the spindle (Abeysuriya et al., 2014). This prediction can be verified by comparing the central frequency of the spindle and the harmonic peaks. However, the frequency resolution of the power spectrum is limited by the short length of sleep spindles. With 256 data points sampled at 200 Hz corresponding to 1.28 s, the resulting power spectrum has a relatively coarse frequency resolution of 0.78 Hz. Therefore choosing the frequency component with largest power is not likely to be an accurate estimate of the peak frequency.

To improve our estimate of the peak frequency, we fit a Gaussian function to the peak and use the center of the Gaussian as the estimate of the peak frequency. The peaks are superimposed on a background spectrum, which introduces a skew to the spectral peak and affects the quality of the Gaussian fit. Following the method developed in previous work (Chiang et al. (2008, 2011)), we perform a power law fit of the form $P = af^b$ over the frequency range where the peak is present to remove background asymmetry in the spectrum before fitting the Gaussian. The parameters and uncertainty of the fit were determined numerically by using a nonlinear Levenberg-Marquardt fitting routine.

2.4. Power relationship

Our model of the brain predicts an approximately quadratic relationship of the power in the spindle harmonic peak to that in the fundamental spindle oscillation (Abeysuriya et al., 2014) so doubling the power of the spindle oscillation is predicted to quadruple the power in the harmonic oscillation.

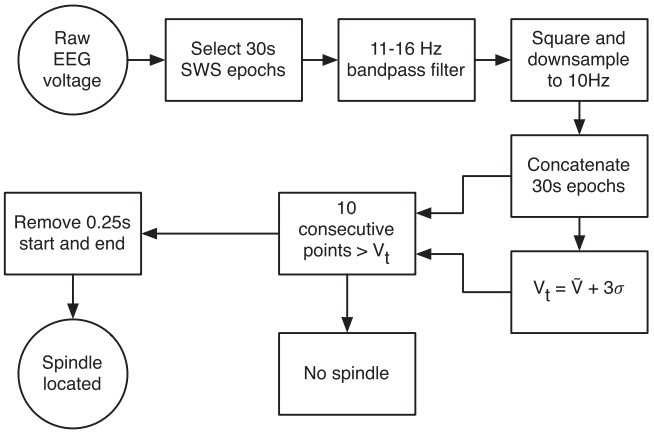

Fig. 3. Schematic outline of method used for automatic spindle detection, as described in the text.

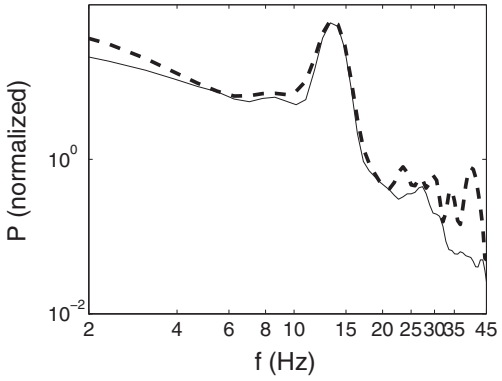

Fig. 4. Spindle power spectrum calculated for all candidate spindle events (dashed) and after artifact rejection (solid), as described in the text. Without spindle artifact rejection, there are significant non-spindle spectral features that obscure the spindle harmonic.

Testing the model prediction requires calculating the power in the peaks in the spectrum corresponding to the spindle oscillation and the harmonic, without background EEG activity. Removal of the background activity is accomplished by performing a power law fit of the form $P = af^b$ from 7–40 Hz, excluding frequencies where peaks are present. This results in an approximation of the baseline background activity over the frequency range where both the spindle and harmonic peaks are present, which can be subtracted from the spectrum to isolate the power in the peaks. The shaded areas in Fig. 5 indicate the power in the spindle peak P_σ and the power in the spindle harmonic P_{σ_2}. The spectrum was interpolated to 0.2 Hz spectral resolution to improve the accuracy of the integration.

The power P_{σ_2} in the spindle harmonic can be considered related to the power P_σ in the fundamental oscillation via

$$P_{\sigma_2} = e^b P_\sigma^m \tag{1}$$

where m is the scaling exponent. The shaded areas in Fig. 5 correspond to P_σ and P_{σ_2}. A linear relationship corresponds to $m = 1$, where doubling P_σ results in doubling P_{σ_2}, while a quadratic relationship corresponds to $m = 2$. In order to determine the scaling exponent in experimental data, we take the logarithm of P_σ and P_{σ_2} and perform a linear fit of the form

$$\log(P_{\sigma_2}) = m\log(P_\sigma) + b, \tag{2}$$

the gradient of the fit yielding the exponent m.

2.5. Bicoherence

One signature of nonlinear effects in a system is a nonrandom phase relationship between oscillations at different frequencies. This can be detected by examining the bicoherence, a quantity that is commonly used to investigate nonlinear coupling between waves in plasmas and other fields, and which has seen recent use in EEG analysis (Pradhan et al., 2012; Sigl and Chamoun, 1994; Venkatakrishnan et al., 2010; Schanze and Eckhorn, 1997; Hayashi et al., 2007). Computing the bicoherence first requires calculation of the bispectrum, which is a complex quantity defined as

$$B(f_1, f_2) = F(f_1)F(f_2)F^*(f_1 + f_2), \tag{3}$$

where B is the bispectrum evaluated at frequencies f_1 and f_2, F is the Fourier transform of the signal, and * denotes the complex conjugate. If the spindle and harmonic waves are nonlinearly coupled, then the phase angle of the bispectrum will have a nonrandom value when evaluated for a large number of spindle events. The bicoherence is an averaged, normalized form of the bispectrum, for which several definitions exist. We define the bicoherence as (Hayashi et al., 2007; Hagihira et al., 2001)

$$b(f_1, f_2) = \frac{|\sum_n B(f_1, f_2)|}{\sum_n |B(f_1, f_2)|}, \tag{4}$$

which is calculated by segmenting a time series into n windows, and calculating the bispectrum separately for each window. The duration of sleep spindles is insufficient to calculate the

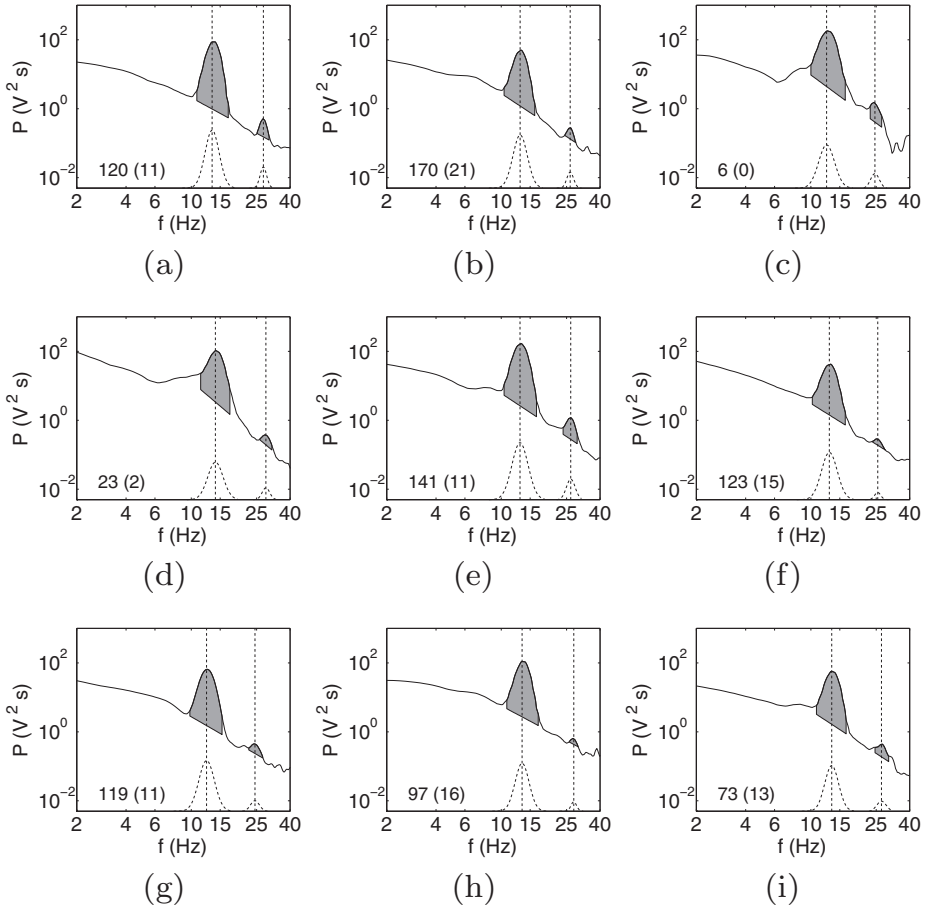

Fig. 5. Power spectra for each of the nine subjects, showing sleep spindles and the spindle harmonic. The dashed vertical lines show the peak frequencies estimated by fitting the Gaussian displayed below the spectrum to the peak. The dashed curves show the fitted Gaussian, which has been offset vertically for clarity. The shaded areas correspond to the integrals used to estimate the power in each peak. The number in the bottom left corner indicates the number of spindle events for each subject, and the number of candidate spindles identified as artifacts is shown in parentheses.

bicoherence for a single spindle event. However, the occurrence of multiple spindle events provides a natural segmentation of the time series. We thus calculate the bicoherence by summation over all the observed spindle events for each subject. If the phase angle of the bispectrum is the same for all the spindle events the bicoherence will equal 1. However, in the limit that the bispectrum phase angle is randomly distributed over a large number of events, the bicoherence approaches zero. Calculating the bicoherence for all pairs of frequencies in the EEG time series enables systematic detection of phase relationships.

The significance of the experimental bicoherence can be tested using surrogate data methods (Schreiber and Schmitz, 2000). For each subject, we construct 100 surrogate data sets by phase randomization of the Fourier transform of each spindle time series, which alters the phase relationships of the Fourier components without changing the linear power spectrum. We use phase randomization rather than more complicated techniques because all of our analysis is performed in the frequency domain, and we do not require reconstruction of the surrogate data time series where changes introduced by phase randomization can be significant. We then calculate the bicoherence for each of the surrogate data sets, which provides the mean bicoherence and standard deviation for each pair of frequencies in the surrogate data where there is no actual phase coupling.

We then determine significance by calculating the difference between the experimental bicoherence and the surrogate data bicoherence in terms of the standard deviation of the surrogate data. If the experimental bicoherence is only a few standard deviations from that of the surrogate data, then it is not significant because it is consistent with random phase coupling for the number of samples present, whereas actual phase coupling results in bicoherence that differs greatly from that of the surrogate data.

3. Results

In all nine subjects, isolation of the sleep spindle events reveals a spindle harmonic at almost exactly double the frequency of the primary peak, as illustrated in Fig. 5. The smoothness of the spectrum depends on the number of spindle events detected. Some subjects have fewer sleep spindles, which results in more noise in the power spectrum (e.g., the subject in Fig. 5c has only six detected spindle events, Fig. 5d has 23 detected spindles, and all of the other subjects have at least 70 detected spindles). However, the size and shape of the harmonic peak depends mainly on the subject (e.g., the subject in Fig. 5a has a relatively large spindle harmonic compared to Fig. 5f, with a similar number of spindles).

The frequency of the primary spindle peak f_σ ranges from 12.4 to 14.0 Hz, and the frequency of the corresponding secondary peak f_{σ_2} ranges from 24.4 to 28.5 Hz. The frequency relationship is maintained even though the primary peak frequency is different in each subject. A 1 Hz shift in the spindle peak is matched by a 2 Hz shift in the secondary peak in all cases, as seen in Fig. 6.

For comparison, the power spectrum predicted by our model is shown in Fig. 7. When the spindle oscillation is strong, a harmonic oscillation is present at double the frequency of the spindle oscillation. The nonlinear origin of the sleep spindle harmonic is verified by linearizing the firing response of the relay nuclei in the model as we showed in our previous study, which abolishes the spindle harmonic without otherwise changing the shape of the spindle peak in the power spectrum (Abeysuriya et al., 2014).

By analyzing the power in the spindle oscillation and in the harmonic across subjects as shown in Fig. 8, we find that the powers satisfy Eq. (1) with $m = 1.6 \pm 0.5$ (95% confidence interval), which is consistent with our theoretical model prediction $m = 2$. Our model predicts that differences in individual physiology will affect the relative power in the spindle and the harmonic, which is a major factor affecting the uncertainty in our estimate of the scaling exponent. This can be addressed by a larger data set with more subjects.

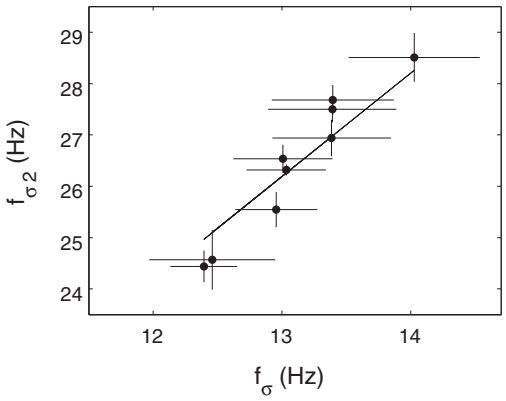

Fig. 6. Fitted frequency of the spindle harmonic peak f_{σ_2} compared to the center frequency of the spindle oscillation f_σ, for each of the nine subjects. The linear fit displayed has $f_{\sigma_2} = af_\sigma$ with $a = 2.01 \pm 0.03$ (95% confidence interval), $R = 0.97$.

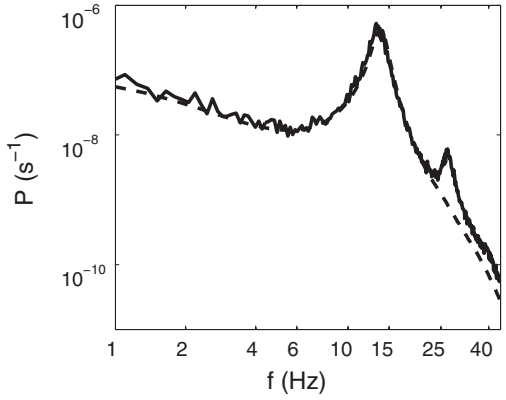

Fig. 7. EEG power spectrum predicted by our model with and without nonlinearity (solid and dashed lines respectively). The sleep spindle harmonic is visible in the power spectrum at around 27 Hz when nonlinearity is present in the model. From Abeysuriya et al., 2014 with permission from Elsevier.

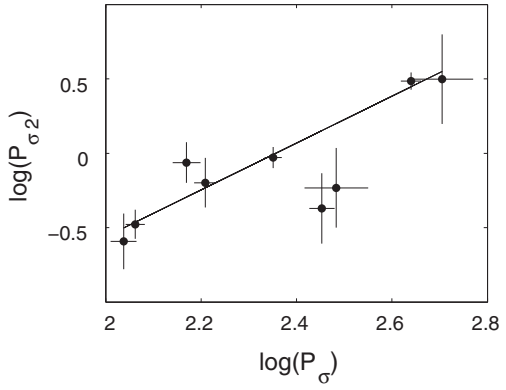

Fig. 8. Power in the spindle harmonic P_{σ_2} relative to power in the primary spindle oscillation P_σ. These powers are shown graphically as shaded areas in Fig. 5. Error bars are computed from upper and lower bounds for the integral based on the uncertainty in each data point. Plotted on a logarithmic scale, the gradient of the linear fit is 1.6 ± 0.5 (95% confidence interval), $R = 0.81$.

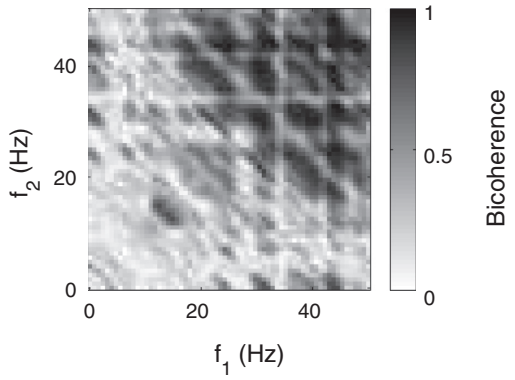

Fig. 9. Raw bicoherence plot for the subject shown in Fig. 5(i). Shading indicates the level of bicoherence observed for each pair of frequencies f_1 and f_2.

All of the subjects showed an increase in bicoherence at the spindle frequency, indicating a phase correlation between the spindle and the harmonic. An example of the raw spectral bicoherence is displayed in Fig. 9. The sleep spindle bicoherence is visible as a dark ellipse oriented along the line $f_1 + f_2 \approx 2f_\sigma$ so that high frequency components of the spindle peak (≈15 Hz) couple with lower frequency components (≈12 Hz) to produce a sharp, narrow spindle harmonic peak.

The raw bicoherence also shows correlations between many other frequences, such as the bicoherence at high frequencies ($f > 30$ Hz) in the upper-right corner of Fig. 9. However, the surrogate data analysis discussed in Section 2 reveals that much of the raw bicoherence is not significant. Fig. 10 shows the difference between the raw bicoherence and the mean surrogate data bicoherence as a multiple of the surrogate data standard deviation, showing frequencies where statistically significant bicoherence is observed. The bicoherence at the spindle frequency is generally 5–15 standard deviations above the surrogate data bicoherence, while other bicoherence features are within 2–3 standard deviations of the surrogate data. This indicates that the bicoherence at the spindle frequency is much more significant than bicoherence at other frequencies. For example, the high frequency bicoherence in Fig. 9 is not significant, as seen in Fig. 10(i). The bicoherence in Fig. 10(c) and (d) is less significant than for other subjects because of the small number of spindle events.

These results are consistent with those from previous studies (Akgül et al., 2000; Venkatakrishnan et al., 2010; Morimoto et al., 2006; Hayashi et al., 2007). Fig. 5(a) and (e) have particularly strong spindle harmonics, and correspondingly significant bicoherence can be observed in Figs. 10(a) and (e). Similarly, the weak spindle harmonic in Fig. 5(f) shows less bicoherence in Fig. 10(f) compared to the other subjects.

Some additional bicoherence can be observed at frequency pairs $(f_1, f_2) = (13, 26), (26, 13)$ Hz in Fig. 10(a), (b), and (e), corresponding to a nonlinear coupling between the spindle oscillation and the harmonic oscillation giving rise to phase-coupled oscillations at around $f_1 + f_2 \approx 39$ Hz. The bicoherence is weaker for this interaction than for the spindle harmonic, and no third harmonic is visible in the power spectrum for any of the subjects. Detection of a possible third harmonic will require significantly larger data sets for each subject in order to reduce the amount of noise in the spectrum.

Finally, moderately significant bicoherence occurs at frequency pairs $(f_1, f_2) = (5, 13), (13, 5)$ Hz in Fig. 10(e–h) corresponding to a

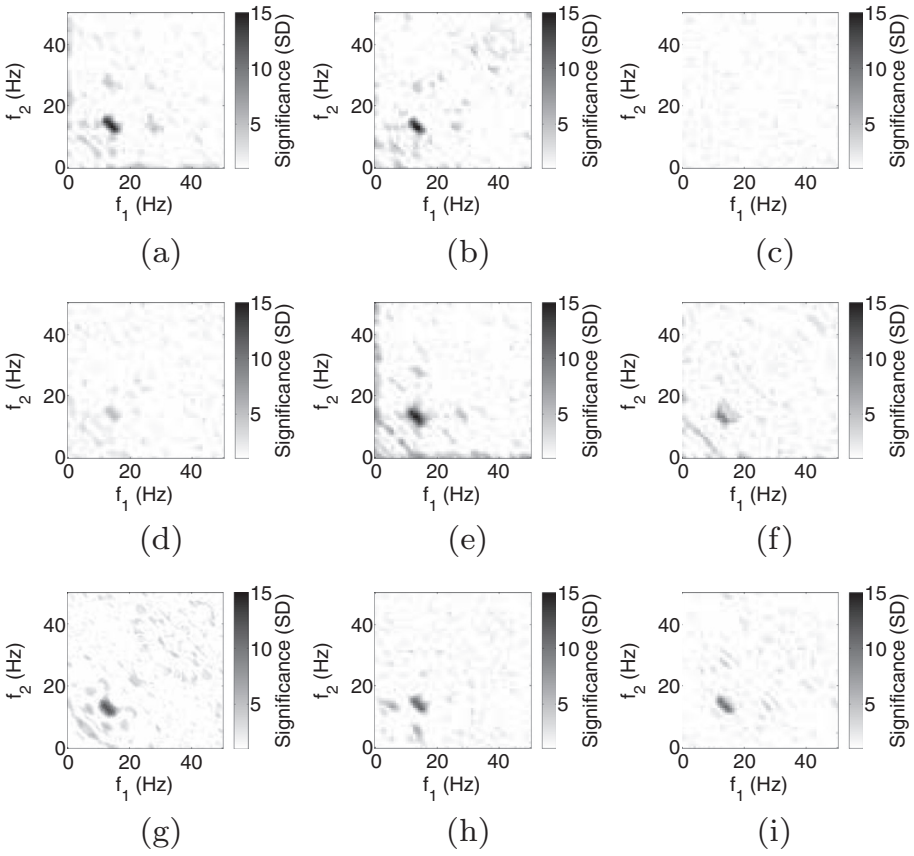

Fig. 10. Bicoherence significance plots for each subject. Shading indicates the difference between the observed bicoherence and the surrogate data bicoherence as a multiple of the standard deviation of a population of 100 surrogate data sets for that subject.

coupling between sleep spindles and theta band oscillations. There do not appear to be any corresponding spectral features in Fig. 5(e–h). However, Laing (2002) observed weak oscillations at 6 Hz accompanying sleep spindles during propofol anesthesia, so based on experimental evidence it is plausible that the sleep spindle mechanism interacts with oscillations in the theta band, although these oscillations may be too weak to observe directly during normal sleep.

4. Discussion

In this study, we examined EEG data from nine subjects to determine whether a sleep spindle harmonic oscillation exists as predicted by a neural field model of the brain that has previously modeled a range of other phenomena (Robinson et al., 2003; O'Connor and Robinson, 2004; van Albada et al., 2010; Rennie et al., 2002; Breakspear et al., 2006; Rowe et al., 2004). We then analyzed the EEG power spectrum and bispectrum to verify the predicted properties of this oscillation. Our main findings are:

(i) A sleep spindle harmonic was observed in all nine subjects at almost exactly double the frequency of the spindle oscillation, as shown by the linear fit $f_{\sigma_2} = (2.01 \pm 0.03) f_\sigma$ in Fig. 6. This strongly suggests that the spindle oscillation and the harmonic oscillation are generated via the same or tightly linked mechanisms.
(ii) Our neural field theory predicts that the spindle harmonic is generated by nonlinear mechanisms during spindle oscillations, rather than being a linear resonance or an independently generated phenomenon. The key signature of the mechanism identified in our theoretical work (Abeysuriya et al., 2014) is that the power P_{σ_2} in the harmonic oscillation should scale quadratically with the power P_σ in the spindle oscillation. The data analyzed in this study yield the consistent result $P_{\sigma_2} \propto P_\sigma^{1.6\pm0.5}$. Tighter bounds for the scaling exponent will require more experimental data.
(iii) Nonlinear generation of the spindle harmonic leads to bicoherence at the spindle frequency, which we observed in the data, reproducing previous experimental results and further strengthening the case for the nonlinear origin of the spindle harmonic. The frequency components containing the spindle oscillation interact with each other to produce the spindle harmonic, and the observed bicoherence was strongest at the predicted frequencies. Bicoherence is intrinsically linked to the shape of the waveform, so bicoherence can appear in the EEG if the waveform has a non-sinusoidal and periodic shape (e.g., triangular and square waves have bicoherence features, with harmonics that scale linearly in power with the fundamental). However, the observed nonlinear power scaling strongly indicates that the observed bicoherence is nonlinear in origin as well.

Multiple phenomena can be responsible for the generation of various peaks in the EEG power spectrum, including so-called "pacemakers" (typically groups of cells with a fixed intrinsic frequency of firing or bursting) and feedback loops between populations. In this study we find that nonlinear effects are responsible for the generation of a sleep spindle harmonic that is predicted to originate in the thalamic relay nuclei (Abeysuriya et al., 2014). This adds to the list of known nonlinear wave dynamics in the brain, including seizures (Robinson et al., 2002; Breakspear et al., 2006) and strong alpha oscillations (Stam et al., 1999; Freyer et al., 2009). However, sleep spindles are an ideal candidate for investigating nonlinear effects in the EEG because they occur in healthy controls, unlike seizures, and do not have a linear delay loop harmonic as occurs for the alpha rhythm (van Albada et al., 2010; Robinson et al., 2001).

The presence of the spindle harmonic in cortical EEG underscores the extent to which neural activity in the thalamic relay nuclei modulates and interacts with activity in the thalamic reticular nucleus. A feedback loop between the reticular nucleus and the relay nuclei (von Krosigk et al., 1993; Bal et al., 1995) is required to produce the harmonic oscillation in our model, and we showed that this delay loop is also able to produce the spindle oscillation itself. There is also some evidence for intrinsic spindle oscillations in the reticular nucleus, which we have previously tested in our model with the result that the intrinsic oscillations are synchronized by the feedback loop (Wu and Robinson, 2007; Wu et al., 2011) as also suggested by Steriade et al. (1985, 1987). Regardless of the mechanism responsible for generating the spindle oscillation itself, the existence of the sleep spindle harmonic highlights the significant role played by the thalamic relay nuclei in generating sleep spindles. Notably, we reiterate that our theory also reproduces other phenomena and provides a unified approach that integrates sleep spindles and the spindle harmonic with previously modeled phenomena under an overall framework.

Acknowledgements

This work was supported by the Australian Research Council, National Health and Medical Research Council (through the Center for Integrated Research and Understanding of Sleep), and the Westmead Millennium Institute.

References

Abeysuriya RG, Rennie CJ, Robinson PA. Prediction and verification of nonlinear sleep spindle harmonic oscillations. J Theor Biol 2014;344:70–7.
Akgül T, Sun M, Sclabassi RJ, Cetin AE. Characterization of sleep spindles using higher order statistics and spectra. IEEE Trans Biomed Eng 2000;47:997–1009.
Bal T, von Krosigk M, McCormick DA. Role of the ferret perigeniculate nucleus in the generation of synchronized oscillations in vitro. J Physiol 1995;483:665–85.
Breakspear M, Roberts JA, Terry JR, Rodrigues S, Mahant N, Robinson PA. A unifying explanation of primary generalized seizures through nonlinear brain modeling and bifurcation analysis. Cerebral Cortex 2006;16:1296–313.
Chiang AKI, Rennie CJ, Robinson PA, Roberts JA, Rigozzi MK, Whitehouse RW, et al. Automated characterization of multiple alpha peaks in multi-site electroencephalograms. J Neurosci Methods 2008;168:396–411.
Chiang AKI, Rennie CJ, Robinson PA, van Albada SJ, Kerr CC. Age trends and sex differences of alpha rhythms including split alpha peaks. Clin Neurophysiol 2011;122:1505–17.
Clemens Z, Fabó D, Halász P. Overnight verbal memory retention correlates with the number of sleep spindles. Neuroscience 2005;132:529–35.
Contreras D, Destexhe A, Sejnowski TJ, Steriade M. Spatiotemporal patterns of spindle oscillations in cortex and thalamus. J Neurosci 1997;17:1179–96.
D'Rozario AL, Kim JW, Wong KKH, Bartlett DJ, Marshall NS, Dijk DJ, et al. A new EEG biomarker of neurobehavioural impairment and sleepiness in sleep apnea patients and controls during extended wakefulness. Clin Neurophysiol 2013;124:1605–14.
Freyer F, Aquino K, Robinson PA, Ritter P, Breakspear M. Bistability and non-Gaussian fluctuations in spontaneous cortical activity. J Neurosci 2009;29:8512–24.
Hagihira S, Takashina M, Mori T, Mashimo T, Yoshiya I. Practical issues in bispectral analysis of electroencephalographic signals. Anesth Analg 2001;93:966–70.
Hamming R. Digital Filters. Englewood Cliffs, New Jersey, USA: Prentice-Hall, 2nd ed.; 1983.
Hayashi K, Tsuda N, Sawa T, Hagihira S. Ketamine increases the frequency of electroencephalographic bicoherence peak on the alpha spindle area induced with propofol. Br J Anaesth 2007;99:389–95.
Laing RJA. A Sleep Spindle Detection Algorithm. Masters thesis, The University of Waikato; 2002.
Li D, Li X, Hagihira S, Sleigh JW. The effect of isoflurane anesthesia on the electroencephalogram assessed by harmonic wavelet bicoherence-based indices. J Neural Eng 2011;8:056011.
McCormick D, Bal T. Sleep and arousal: thalamocortical mechanisms. Annu Rev Neurosci 1997;20:185–215.
Morimoto Y, Hagihira S, Yamashita S, Iida Y, Matsumoto M, Tsuruta S, et al. Changes in electroencephalographic bicoherence during sevoflurane anesthesia combined with intravenous fentanyl. Anesth Analg 2006;103:641. 5.

Niedermeyer E, Lopes da Silva FH. Electroencephalography: basic principles, clinical applications, and related fields. M - Medicine Series. Baltimore. 4th ed. Maryland, USA: Lippincott Williams & Wilkins; 1999.
O'Connor SC, Robinson PA. Spatially uniform and nonuniform analyses of electroencephalographic dynamics, with application to the topography of the alpha rhythm. Phys Rev E 2004;70:11911.
Pradhan C, Jena SK, Nadar SR, Pradhan N. Higher-order spectrum in understanding nonlinearity in EEG rhythms. Comput Math Methods Med 2012;2012:206857.
Rennie CJ, Robinson PA, Wright JJ. Unified neurophysical model of EEG spectra and evoked potentials. Biol Cybern 2002;86:457–71.
Robinson PA, Rennie CJ, Rowe DL. Dynamics of large-scale brain activity in normal arousal states and epileptic seizures. Phys Rev E 2002;65:41924.
Robinson PA, Rennie CJ, Rowe DL, O'Connor SC. Estimation of multiscale neurophysiologic parameters by electroencephalographic means. Hum Brain Mapp 2004;23:53–72.
Robinson PA, Rennie CJ, Rowe DL, O'Connor SC, Gordon E. Multiscale brain modelling. Philos Trans R Soc Lond Ser B 2005;360:1043–50.
Robinson PA, Rennie CJ, Rowe DL, O'Connor SC, Wright JJ, Gordon E, et al. Neurophysical modeling of brain dynamics. Neuropsychopharmacology 2003;28(Suppl 1):S74–9.
Robinson PA, Rennie CJ, Wright JJ, Bahramali H, Gordon E, Rowe DL. Prediction of electroencephalographic spectra from neurophysiology. Phys Rev E 2001;63:21903.
Robinson PA, Whitehouse RW, Rennie CJ. Nonuniform corticothalamic continuum model of electroencephalographic spectra with application to split-alpha peaks. Phys Rev E 2003;68:21922.
Rosner B. Percentage points for a generalized ESD many-outlier procedure. Technometrics 1983;25:165–72.
Rowe DL, Robinson PA, Harris AW, Felmingham KL, Lazzaro IL, Gordon E. Neurophysiologically-based mean-field modelling of tonic cortical activity in post-traumatic stress disorder (PTSD), chronic schizophrenia, first episode schizophrenia (FESz) and attention deficit hyperactivity disorder (ADHD). J Integr Neurosci 2004;3:453–87.
Rowe DL, Robinson PA, Rennie CJ. Estimation of neurophysiological parameters from the waking EEG using a biophysical model of brain dynamics. J Theor Biol 2004;231:413–33.
Saletin JM, Goldstein AN, Walker MP. The role of sleep in directed forgetting and remembering of human memories. Cereb Cortex 2011;21:2534–41.
Schabus M, Gruber G, Parapatics S, Sauter C, Klösch G, Anderer P, et al. Sleep spindles and their significance for declarative memory consolidation. Sleep 2004;27:1479–85.
Schanze T, Eckhorn R. Phase correlation among rhythms present at different frequencies: spectral methods, application to microelectrode recordings from visual cortex and functional implications. Int J Psychophysiol 1997;26:171–89.
Schreiber T, Schmitz A. Surrogate time series. Phys D: Nonlinear Phenom 2000;142:346–82.
Sigl J, Chamoun N. An introduction to bispectral analysis for the electroencephalogram. J Clin Monit Comput 1994;10:392–404.
Stam CJ, Pijn JPM, Suffczynski P, Lopes da Silva FH. Dynamics of the human alpha rhythm: evidence for non-linearity? Clin Neurophysiol 1999;110:1801–13.
Steriade M, McCormick DA, Sejnowski T. Thalamocortical oscillations in the sleeping and aroused brain. Science 1993;262:679–85.
Steriade M, Deschênes M, Domich L, Mulle C, Deschenes M. Abolition of spindle oscillations in thalamic neurons disconnected from nucleus reticularis thalami. J Neurophysiol 1985;54:1473–97.
Steriade M, Domich L, Oakson G, Deschênes M. The deafferented reticular thalamic nucleus generates spindle rhythmicity. J Neurophysiol 1987;57:260–73.
van Albada SJ, Kerr CC, Chiang AKI, Rennie CJ, Robinson PA. Neurophysiological changes with age probed by inverse modeling of EEG spectra. Clin Neurophysiol 2010;121:21–38.
Venkatakrishnan P, Sukanesh R, Sangeetha S. Detection of quadratic phase coupling from human EEG signals using higher order statistics and spectra. SIViP 2010;5:217–29.
von Krosigk M, Bal T, McCormick D. Cellular mechanisms of a synchronized oscillation in the thalamus. Science 1993;261:361.
Wolter S, Friedel C, Böhler K, Hartmann U, Kox WJ, Hensel M. Presence of 14Hz spindle oscillations in the human EEG during deep anesthesia. Clin Neurophysiol 2006;117:157–68.
Wu H, Robinson PA. Modeling and investigation of neural activity in the thalamus. J Theor Biol 2007;244:1–14.
Wu HY, Robinson PA, Kim JW. Firing responses of bursting neurons with delayed feedback. J Comput Neurosci 2011;31:61–71.
Yu RC, Teh HW, Jaques PA. Sioutas C, Froines JR., Quality control of semi-continuous mobility size-fractionated particle number concentration data. Atmos Environ 2004;38:3341–8.